

# Estimation of Fracture Surface Area based on Tracer and Temperature Histories

Anna Suzuki<sup>1,2</sup>

<sup>1</sup>Institute of Fluid Science, Tohoku University

<sup>2</sup>Energy Resources Engineering, Stanford University

## Keywords

*Tracer, temperature, optimization, fracture surface area*

## ABSTRACT

In EGS reservoirs, a fracture surface area is one of key uncertainty in development. We propose a method to estimate cumulative fracture surface area for each multiple flow path based on tracer and temperature data with cold water injection. Tracer response is used to obtain the flow properties and determine the pore volume for each flow path. By substituting the pore volumes, analytical solutions of heat transfer equation can consist of measurable and/or controllable properties except fracture surface area for each path. The unknown fracture surface areas are estimated by comparison between the superposition of analytical solutions of heat transfer equations and observed temperature decline. Validation with numerical simulation results suggests that even though the number of flow paths is unknown, use of “virtual flow path” can estimate the pore volumes and fracture surface areas. For the simulation results, temperature history for 28 days (10% of temperature decline) provides reasonable estimation of fracture surface area with error of 15.0%.

## 1. Introduction

Enhanced Geothermal Systems (EGS) injects cold water into fractures in hot rock to “mine” the heat from the rock. The EGS performance should be predicted at the early stage of development, which relies on thermal properties of the rocks (heat capacity, thermal diffusivity, etc.), conditions of the injected water (position, temperature, flow rate), and the fracture structures. The thermal properties are measurable. Although the thermal properties depend on temperature, thermal performance can be predicted with small errors by using constant properties (Stopa and Wojnarowski, 2006). The conditions of the injected water are controllable in the development strategy. Thus, a key uncertainty is the fracture structures that controls the rate of heat transfer between the host rock and the circulating injected water.

Carslaw and Jaeger (1959) show analytical solutions for heat exchangers with 1-D flow in the “fracture” and no flow in the “matrix.” Robinson and Tester (1984) and Robinson et al. (1988)

used similar equations in matching production temperature histories for two EGS projects by adjusting the surface area of the single fracture. Their models need to determine fracture thickness, and the assumption of the single fracture with 1D flow normally oversimplifies complex reservoir structures. Shan and Pruess (2005) use a 2-D geometry with uniform flow per fracture to show that specific surface area can be estimated using a diffusing tracer. Pruess and Doughty (2010) show that matching huff-n-puff tests using temperature as a tracer is useful to estimate changes in heat transfer area but show no explicit calculation for surface area. Although cation exchange was used to estimate fracture surface area (Dean et al., 2015), the method relies on the accuracy of the reservoir properties used in the simulation. Robinson and Tester (1984) showed a relationship between heat exchange surface area and reservoir volume for two EGS reservoirs. This correlation demonstrates the need to estimate both fracture volume and surface area to optimize EGS heat extraction over reservoir life.

Previous work proposed a Work Flow to estimate fracture surface area by using tracer and temperature histories (Shook and Suzuki, 2017). We first analyze tracer response data to estimate the fracture pore volume, the flow geometry, and the number of fractures. Substituting these values into the heat transfer equations, the fracture surface area is estimated. The method can estimate fracture surface area reasonably for cases of a uniform fracture and three distinguished flow paths. The purpose of this paper is to generalize the method for multiple flow paths whose number is unknown. The paper briefly explains the modified method and verify the method by using the same simulation data used in Shook and Suzuki (2017).

## 2. Method of Surface Area Estimation

We estimate fracture surface areas between an injection well and a production well through an operation of cold water injection. The Work Flow of estimating fracture surface areas is described in Figure 1. We assume that water and tracer at lower temperature than the reservoir are injected into an injection well. The tracer concentration and temperature decline curve are observed at a production well. The flow rate is assumed to be constant, and it is also assumed that no water has leaked into the surrounding rocks. The tracer breakthrough curve is used for obtaining flow, which is then substituted into heat transfer equations. The analytical solutions of the heat transfer equations are compared with the thermal drawdown data. Then, we can optimize the fracture surface area. The details are explained as follows.

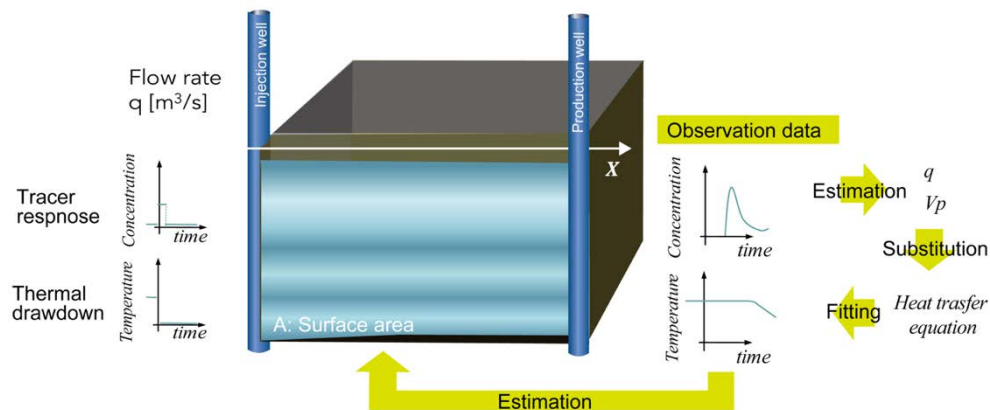


Figure 1: Estimation of fracture surface area based tracer and temperature.

## 2.1 Determination of flow rate and pore volume from tracer response

Flow capacity – storage capacity diagrams (F-C diagrams) have appeared in petroleum reservoir engineering literature for decades (Stiles, 1949; Schmalz and Rahme, 1950; Lake, 1989; Gunter et al., 1997). Shook and Forsmann (2005) and Shook et al. (2009) generalized F-C curves to use dynamic data (e.g. tracers) and termed this the dynamic F- $\Phi$  curve. The F- $\Phi$  curve can be estimated from tracer data, and the flow capacity at data point  $n$ ,  $F_n$ , and storage capacity  $\Phi_n$  are given by

$$F_n = \frac{\sum_{i=1}^n c_i \Delta t_i}{\sum_{i=1}^{N_{tot}} c_i \Delta t_i} \quad (1)$$

$$\Phi_n = \frac{\sum_{i=1}^n c_i t_i \Delta t_i}{\sum_{i=1}^{N_{tot}} c_i t_i \Delta t_i} \quad (2)$$

where  $N_{tot}$  is the total number of data points.  $c_i$  is the tracer concentration at  $i$  th data.  $t_i$  is the time at  $i$  th data.  $\Delta t_i$  is the time difference at  $i$  th data. The total of flow capacity and storage capacity are 1 ( $F_{N_{tot}} = 1$  and  $\Phi_{N_{tot}} = 1$ ). F-  $\Phi$  curves are used qualitatively and quantitatively, for example “60% of the flow is coming from 12% of the pore volume.”

We also consider that the F- $\Phi$  curve is simply a cumulative curve of the fractions of capacities for individual flow paths. When the number of flow path is  $N_{flow}$ , the fractions of the flow capacity for  $j$  th flow path,  $f_j$ , and the fraction of the storage capacity,  $\varphi_j$ , are given by the F-  $\Phi$  curve as

$$\sum_{j=1}^{N_{path}} f_j = \sum_{j=1}^{N_{path}} (F_j - F_{j-1}) = 1 \quad (3)$$

$$\sum_{j=1}^{N_{path}} \varphi_j = \sum_{j=1}^{N_{path}} (\Phi_j - \Phi_{j-1}) = 1 \quad (4)$$

where  $F_j$  is the flow capacity until the data point for the  $j$  th flow path.  $\Phi_j$  is the storage capacity until the data point for the  $j$  th flow path. The fractions of flow rate for  $j$  th flow path can be given as

$$q_j = f_j q_{tot} \quad (5)$$

where  $q_{tot}$  is the total flow rate. The total flow rate is set to the production rate multiplied by the reservoir porosity. The  $j$ th pore volume  $V_{pj}$  is approximated as the product of the production rate  $q_{tot}$  multiplied by the fraction of storage capacity  $\varphi_j$  and the average travel time  $\tau_j$  as

$$V_{pj} = q_j \tau_j \quad (6)$$

where  $\tau_j$  is calculated by the tracer response as

$$\tau_j = \frac{\sum_{n_{j-1}}^{n_j} c_i t_i \Delta t_i}{\sum_{n_{j-1}}^{n_j} c_i \Delta t_i} \quad (7)$$

where  $n_j$  is the data point associated to  $j$  th flow path.

The number of flow paths might be recognized from tracer responses in the case where the flow paths are completely separated. Shook and Suzuki (2017) shows that the proposed method can be applied to the case of three flow paths. Since there were obvious three difference of gradient in the  $F-\Phi$  curve, they segmented the flow capacity and the storage capacity into three fractions and obtained three fractions of pore volume. In reality, the flow paths are not always separated, and tracer response does not show obvious peaks if the permeability varies continuously. For instance, permeability in fault zones varies spatially, and the tracer response shows gradual declines (Suzuki et al., 2016). In order to generalize the estimation, this study aims at improving the method in which the number of flow paths is not determined. In this way, we set “virtual flow paths” and obtain each fraction of flow rate and each fraction of pore volume due to the number of the virtual flow paths. Determination of the ratios of flow capacity and storage capacity are also forced to subjective judgement. Thus, we equally divide the flow capacity and determine the storage capacity associated with it from the  $F-\Phi$  curve, as shown in Figure 2. This is expected to lead to estimation for uncountable flow paths.

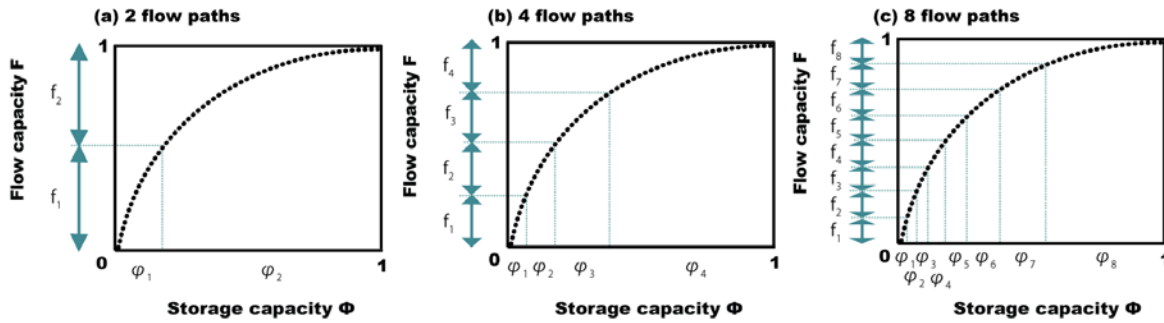


Figure 2: Even fractions of flow capacities and the storage capacities associated with the flow capacities.

## 2.2 Analytical solution of heat transfer equation

The governing equations in Gringarten and Sauty (1975), which are similar to that by Lauwerier (1955) and Carslaw and Jaeger (1959), can be written for flow in a fracture with conduction of heat in the surrounding rock:

$$\frac{b}{2}(\rho C_p)_T \frac{\partial T_w}{\partial t} + \frac{q}{2}(\rho C_p)_w \frac{\partial T_w}{\partial S} - K_R \frac{\partial T_R}{\partial z} \Big|_{z=b/2} = 0 \quad (8)$$

for the fracture (see Nomenclature for a definition of variables) with  $(\rho C_p)_T = \phi(\rho C_p)_w + (1-\phi)(\rho C_p)_R$ . The surrounding rock matrix temperature is governed by the following equation:

$$\frac{(\rho C_p)_R}{K_R} \frac{\partial T_R}{\partial t} - \frac{\partial^2 T_R}{\partial z^2} = 0 \quad (9)$$

The temperatures also satisfy the following initial and boundary conditions:

$$T_w(S, t) = T_R(S, z, t) = T_I, \quad t \leq \frac{\phi b S}{q}; \quad (10a)$$

$$T_w(0, t) = T_I, \quad t > 0; \quad (10b)$$

$$T_w(S, t) = T_R(S, b/2, t), \quad \forall S, t; \quad (10c)$$

$$\lim_{z \rightarrow \infty} T_R(S, z, t) = T_I, \quad \forall S, z, t; \quad (10d)$$

Gringarten and Sauty (1975) show the solution of Eqs. (8) and (9), subject to constraints Eq. (10), is

$$\frac{T_I - T_w(t)}{T_I - T_J} = \operatorname{erfc} \left[ \frac{(\rho C_p)_w}{K_R (\rho C_p)_R} \left( \frac{q}{S} \right)^2 \left\{ t - \frac{(\rho C_p)_T}{(\rho C_p)_w} \frac{bS}{q} \right\} \right]^{1/2} \quad (11)$$

We use the following identities in terms the surface area of the fracture:

$$V_p = bWL\phi = bS\phi, \quad (12)$$

$$A = 2S. \quad (13)$$

We get

$$T_w(L, t) = T_I - (T_I - T_J) \operatorname{erfc} \left[ \frac{1}{(\rho C_p)_w} \frac{A}{2q} \sqrt{K_R (\rho C_p)_R} \frac{1}{\left( t - \frac{(\rho C_p)_T}{(\rho C_p)_w} \frac{V_p}{\phi q} \right)^{1/2}} \right], \quad (14)$$

where  $K_R$  is the thermal conductivity of the rock, and  $\phi$  is the porosity, which can be determined from the measurement. Thus, Eq. (14) is a function as  $T_w = T_w(L, t, A, q, V_p)$ .

### 2.3 Curve fitting to observed temperature data

We consider the temperature decline occurs for each flow path and the total decay is the superposition of the temperature, weighted by the fraction of flow rate in the following form:

$$T_w(t) = \frac{1}{q_{tot}} \sum_{j=1}^{N_{path}} q_j w_{wj}(L, t, A_j, q_j, V_{pj}), \quad (15)$$

where  $V_{pj}$  and  $q_j$  is obtained from the tracer breakthrough curve, explained in the previous section. Therefore, unknown parameters in Eq. (15) are the fracture surface areas for each flow path,  $A_j$ . Optimization is conducted by curve fitting between Eq. (15) and observation data of temperature history, which provides the fractions of surface area for each flow path. The fractions of surface area are added up to obtain the total.

### 3. Numerical Simulation for Verification

We used TOUGH2 (Pruess, 1991) to simulate the reservoir response and calculate tracer and temperature histories. An acceptable comparison of surface area validates the proposed method and gives us confidence in predicting the performance of the EGS reservoir. Of course, these predictions are only valid for the specific reservoir properties. Other simulations would be needed for a specific EGS field test.

The model used for this study was a single well pair completed in a single vertical fracture set in non-fractured native rock. We assume the fracture permeability is a constant  $1.0 \times 10^{-11} \text{ m}^2$  ( $\sim 10$  D). The second example is one single fracture surrounded by two damage zones, that is, three flow paths exist.

The half-length of the fracture was set to 99 m with a height of 75 m and an aperture of 0.02 m. The matrix width was 642.66 m to ensure semi-infinite media over the time scale of interest, with grid block sizes increasing by a factor of 2 away from the fracture to ensure numerical error was controlled. The wells are completed only in the fracture. Figure 3 shows a schematic of the model. Thermal and physical properties of the rock were taken from the literature and are summarized in Table 1. The matrix is assumed to have no permeability.

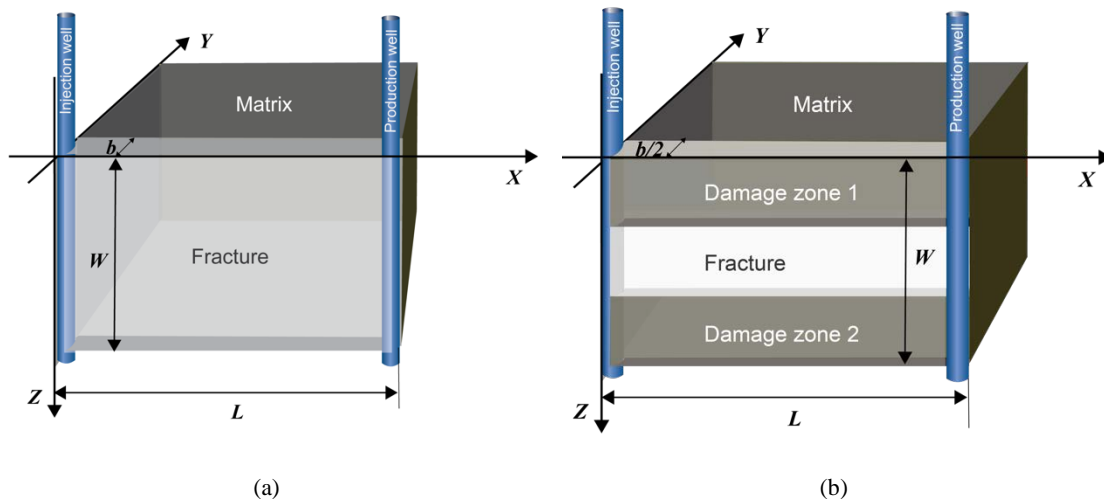


Figure 3: A schematic of the EGS reservoir:(a) uniform fracture and (b) three flow paths (a fracture surrounded by two damage zones).

**Table 1: Simulation properties inTOUGH2.**

$\rho_R$ (kg/m <sup>3</sup> )	2569		Single fracture	Three flow paths	
$C_{pR}$ (J/kg C)	803	$\phi$	0.9	DZ 1	0.75
$K_R$ (W/m C)	2.569			Fracture	0.5
$\rho_w$ (25 C) (kg/m <sup>3</sup> )	997.1			DZ 2	0.95
$\rho_w$ (200 C) (kg/m <sup>3</sup> )	864	Permeability (10 <sup>-12</sup> m <sup>2</sup> )	10	DZ 1	4
$C_{pw}$ (25 °C) (J/kg K)	4180			Fracture	10
$C_{pw}$ (200 °C) (J/kg K)	4510			DZ 2	2
$P_I$ (kPa)	9800	$V_p$ (m <sup>3</sup> )	125.55	DZ 1	34.875
$T_I$ (°C)	200			Fracture	23.25
$q_{tot}$ (kg/s)	2			DZ 2	44.175
$T_J$ (°C)	25	$A$ (m <sup>2</sup> )	13950	DZ 1	4650
Model dimensions (m)	99 × 75 × 643			Fracture	4650
Grid dimensions	33 × 15 × 3			DZ 2	4650
$\Delta X$ (m)	3				
$\Delta Y$ (m)	0.01, 0.02, 0.04, ...				
$\Delta Z$ (m)	25				

The initial temperature is 200 °C, and the initial pressure was set to 9800 kPa, about the hydrostatic pressure gradient assuming the fracture is at 1 km depth. At  $t = 0$ , water at 25 °C was injected for 1 hour, followed with 25 °C water with 10% tracer for one hour and then with 25 °C water without tracer for the balance of the simulation. All injection and production rates were 2 kg/s. For reasons of symmetry we simulated a half-space solution, but the results showed below are for the full solution for a single well pair with surrounded rocks.

#### 4. Numerical Results

The tracer responses and temperature histories for cases of (a) a uniform single fracture and (b) three flow paths were obtained from TOUGH2. Tracer responses are shown in Figures 4(a)(b). The tracer response for the case of the uniform fracture shows a bell-shaped distribution, while the curve for the three flow paths exhibits three peaks. We easily recognize that there were three flow paths with different flow rate.

The tracer responses were used to obtain the F-  $\Phi$  plots shown in Figures 4(c)(d). The greater the deviation of this curve from the 45° degree line the greater the heterogeneity of the system.

The F-  $\Phi$  plot for the case of uniform fracture in Figure 4(c) is close to the 45° degree line, which suggests that the flow system is homogeneous. The F-  $\Phi$  plot for the case of three flow paths shows a kink at  $f$  of 0.6 and  $\Phi$  of 0.23. This indicates that 60% of flow came from 23% of the pore volume. The previous paper used this point and another point at  $f$  of 0.89 and  $\Phi$  of 0.63 and separated into three flow paths (Shook and Suzuki, 2017). We show that the method provides successful estimation of fracture surface area.

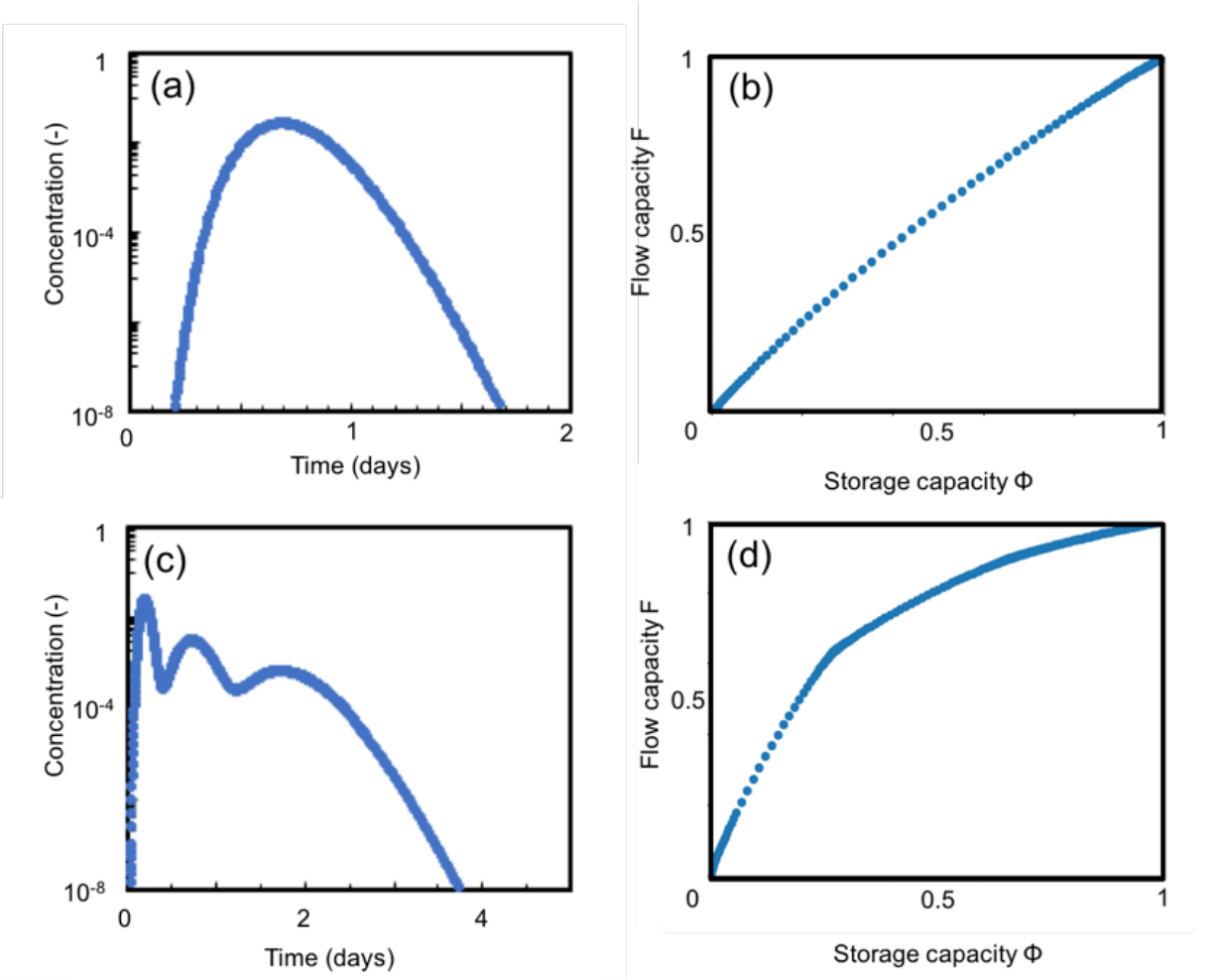


**Figure 4. Tracer histories for (a) uniform fracture and (b) three flow paths and F- $\Phi$  curves for (c) uniform fracture and (d) three flow paths.**

As mentioned in above, this paper aims at proposing a method for unknown or uncountable flow path. We set “virtual flow paths” and divided flow capacity into a certain division number. Figures 5(a)(b) shows the fractions of the flow capacity for different division numbers. The division number varied from 1 to 10. The different colors indicate each fraction of flow capacity. Because we equally divided the flow capacity, the fractions of flow capacity were same for each division number. Fractions of the flow rate were determined by the fraction of the flow capacity. The ratio of the flow rate is also plotted in the y-axis on the right side in Figures 5(a)(b).

Once we divide the flow capacity into the fraction, the fractions of storage capacity are determined by the F-  $\Phi$  plot. Figures 5(c)(d) shows the fractions of the storage capacity for different division numbers. Compared to the equal divisions for the fractions of the flow capacity, the fractions of storage capacity show different ratios. Especially, the trend for the case of three flow paths is more obvious than for the case of uniform fracture. For instance, in the case of the division number of 2, the flow capacity is separated into 2 fractions, which means  $f_1 = 0.5$  and  $f_2 = 0.5$  for both cases. Then, the fractions of the storage capacity were determined as  $\phi_1 = 0.45$  and

$\varphi_2 = 0.55$  for the case of uniform fracture, while as  $\varphi_1 = 0.21$  and  $\varphi_2 = 0.79$  for the case of three flow paths.

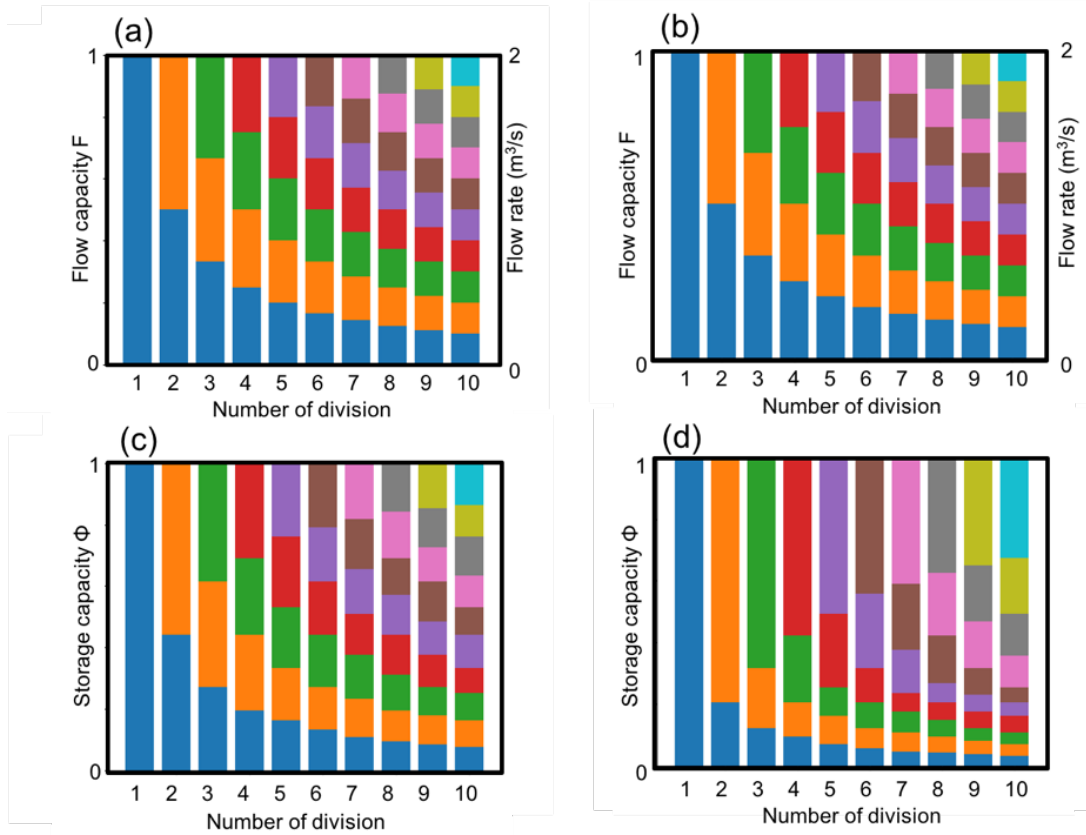


**Figure 5. Flow capacities and fractions of flow rate for (a) uniform fracture and (b) three flow paths, and storage capacities for (c) uniform fracture and (d) three flow paths.**

The travel times for each flow path were calculated by Eq. (7) and used to estimate pore volume in Eq. (6). Figure 6 shows the estimated pore volume for different division numbers. Since the true pore volume is  $133.65 \text{ m}^3$  and  $108.9 \text{ m}^3$  for the case of uniform fracture and the three flow paths, the errors were less than 3.3% and 2.4%, respectively. We found that the number of division of flow paths does not have large effect on the estimation of pore volume and that estimation of pore volumes by Eq. (6) is reasonable.

Substituting the fractions of the flow rate  $q_j$  and the fractions of the pore volume  $V_{pj}$  into Eq. (13), the solution of Eq. (13) were compared with the temperature history simulated by TOUGH2. We used the temperature decreasing by 70%, 20%, 10%, and 5% of the difference between the initial temperature and the injection temperature. Since the difference between the initial temperature and the injection temperature was  $175 \text{ }^\circ\text{C}$ , “5% decline” means that the temperature data is from  $200 \text{ }^\circ\text{C}$  to  $191.25 \text{ }^\circ\text{C}$ . Figure 7 shows the temperature decline curve for the case of three flow paths.

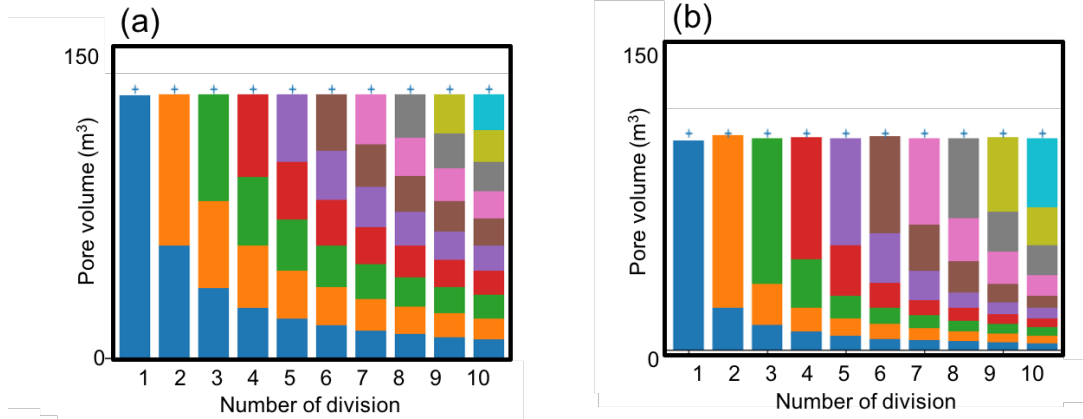


Figure 6. Estimated pore volumes for the case of (a) uniform fracture and (b) three flow paths. Exact answer is plotted as ‘+’.

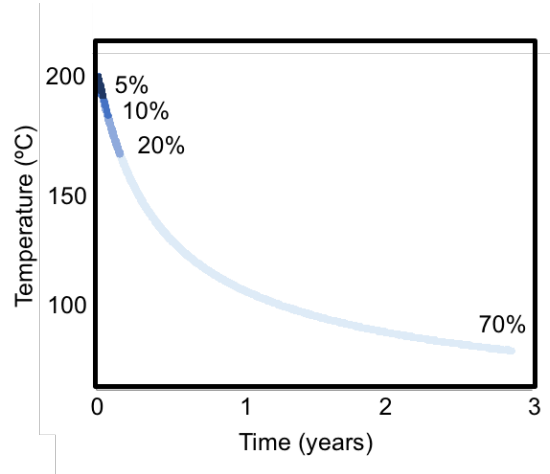
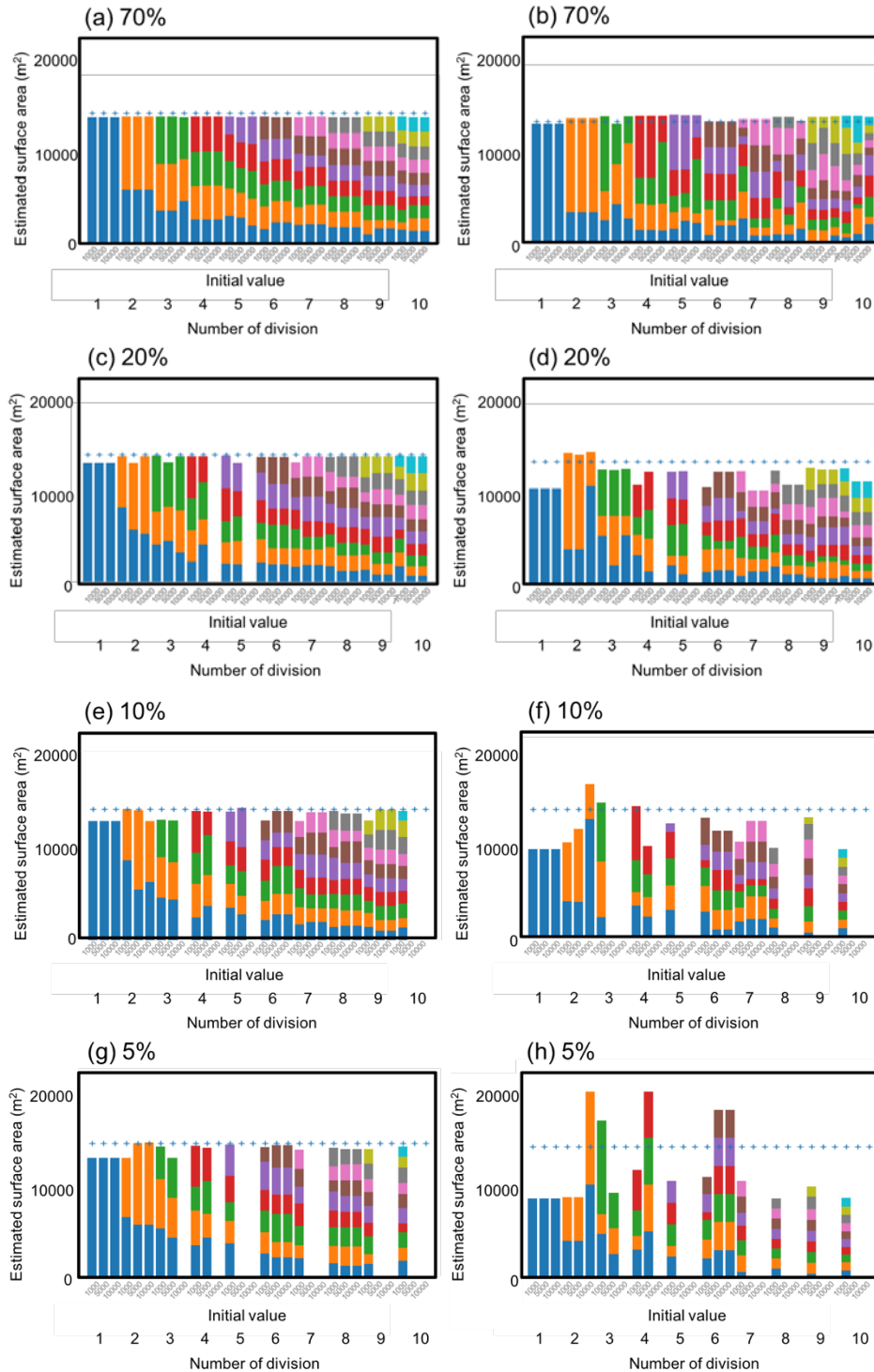


Figure 7: Temperature history for three flow paths simulated by TOUGH2.

The fractions of the surface area  $A_j$  were the optimized parameters. The objective function was the difference between the simulated and predicted values, and values for each fraction of surface area  $A_j$  were optimized to minimize the objective function by the L-BFGS-B method in python function. For optimization, we set three different initial values of the fraction of surface area  $A_j$  as 1000, 5000, and 10000. Figure 8 shows the estimated results for fracture surface area. The true value of surface area was  $13950 \text{ m}^2$ , plotted as “+”. Each number of division used three initial values. The different colors describe the fractions of surface area. The estimated surface area is the total of the fractions. The estimation results using 70%, 20%, 10%, and 5% temperature declines are plotted by separately in Figure 8. If the optimization does not converge, the result was not plotted.



**Figure 8: Estimated fracture surface area for (a)(c)(e)(g) uniform fracture and (b)(d)(f)(h) three flow paths with three different initial values (1000, 5000, and 10000) for optimization. Optimization was conducted using temperature decreasing by (a)(b) 70%, (c)(d) 20%, (e)(f) 10%, and (g)(f) 5% of the difference between the initial temperature and the injection temperature, respectively. “+” is the exact answer.**

When we changed the initial values for the fractions of surface area  $A_j$ , the fractions of surface area  $A_j$  could vary as shown in Figure 8. However, the total surface areas estimated by using 70% decline were almost same for the case of uniform fracture (Figure 8(a)) and gave the errors of around 2%. These results indicate that the optimization does not depend on the initial values for optimization and also the number of division of flow properties. In contrast, for the case of three flow paths (Figure 8(b)), the estimated values by using 70% decline differ for initial values for optimization and the number of division. Yet, the errors were in the range between 1% and 6%. When the number of division was one, that is, assuming a single fracture, the estimation was worst. This implies that the estimation with a single fracture could underestimate.

When we used less data for the optimization (i.e., 20%, 10% and 5% temperature decline as shown in Figures 8(c)-(h)), there were some cases where the optimization did not converge. Further study needs to find reasonable optimization methods. We calculated the average of the estimations for different percentage of temperature data. That is, the average was from the estimated values with 3 different initial values and with the 10 different numbers of division of flow paths, except the case where the optimization did not converge. The errors of the average estimations are shown in Figure 9. The case of uniform fracture produced less error than the case of the three flow paths. Less temperature decline data led to larger errors. When we used 5% of temperature decline curves, the estimation error was 31.5%, which was not small error. However, when we used 10% of temperature decline curves, the estimation error decrease to 15.8%. In this simulation (i.e., 100 m scale fracture), it took 28 days to obtain 10% decline of the temperature. If we could estimate the fracture surface area with such premature temperature decline, strategic development can be done. Although there is an obvious kink in the F- $\Phi$  curve for the three paths in Figure 4(d), we neglected the trend but set the fractions of the flow capacity evenly. Nonetheless, this method led to the reasonable estimations of total surface area with premature temperature decline.

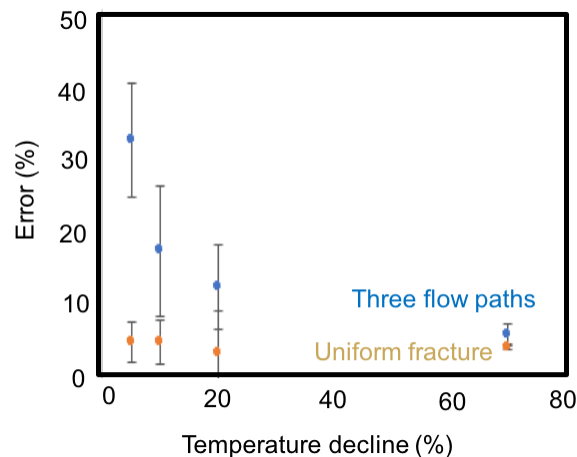


**Figure 9: Estimated errors of surface area for different ratios of temperature decline data.**

## 5. Summary and Conclusions

We have presented a Work Flow that uses analytic solutions to estimate surface area available for heat conduction to working fluid in EGS environments. The novel contribution of the work

was to write the solution of temperature decline curve with measured or controlled parameters except fracture surface area. Even though the number of flow paths is not distinguished, we could apply this estimation. Tracer response was used to describe the  $F-\Phi$  plot, which provided the fractions of flow rate and the fraction of the pore volume for each flow path. Shook and Suzuki (2017) shows how to use the Work Flow to estimate power generation as a function of fracture properties (measured) and flow rates (controlled), and discuss how to scale up to multiple production wells and “fracture packs.” This Work Flow would be useful for EGS reservoir development.

## ACKNOWLEDGEMENTS

The author is pleased to thank Mike Shook for great knowledge about analyzing tracer and temperature data. This work was supported by the JSPS KAKENHI Grant Number 717H049760, whose support are gratefully acknowledged. All data for this paper are properly cited and referred to in the reference list. The source code and the fracture data for Appendix A are properly cited and referred to in the reference list. All experimental data are available from the authors upon request ([anna.suzuki@tohoku.ac.jp](mailto:anna.suzuki@tohoku.ac.jp)).

## NOMENCLATURES

$A$	Total surface area [ $\text{m}^2$ ]
$A_j$	Surface area of the $j$ th flow path [ $\text{m}^2$ ]
$b$	Half aperture of the fracture [m]
$c_i$	Concentration of tracer at data point $i$ [ $\text{kg}/\text{m}^3$ ]
$C_p$	Heat capacity (i=water w, but rock, R) [ $\text{J}/\text{kg}/\text{K}$ ]
$F_n$	Cumulative flow capacity at data point $n$
$f_j$	Flow capacity of the $j$ th flow path
$K_R$	Thermal conductivity of the rock [ $\text{W}/\text{m}/\text{K}$ ]
$L$	Minimum spacing between “fracture packs” [m]
$n_j$	Data point associated to $j$ th flow path
$N_{path}$	Total number of flow paths
$N_{tot}$	Total number of data points
$P_I$	Initial pressure [Pa]
$q$	Volumetric flow rate [ $\text{m}^3/\text{s}$ ]
$q_{tot}$	Volumetric total production rate [ $\text{m}^3/\text{s}$ ]
$q_j$	Volumetric flow rate of the $j$ th flow path [ $\text{m}^3/\text{s}$ ]

$S$	Surface area of the fracture [ $\text{m}^2$ ]
$t$	time [s]
$t_i$	time at data point $i$ [s]
$\Delta t_i$	Discretized time at data point $i$ [s]
$T_{wj}$	Temperature of the $j$ th flow path [ $^{\circ}\text{C}$ ]
$T_I$	Initial temperature [ $^{\circ}\text{C}$ ]
$T_J$	Injected temperature [ $^{\circ}\text{C}$ ]
$T_R$	Temperature in the surrounding rock matrix [ $^{\circ}\text{C}$ ]
$T_w$	Temperature in the fracture [ $^{\circ}\text{C}$ ]
$V_p$	Total pore volume [ $\text{m}^3$ ]
$V_{pj}$	Pore volume of the $j$ th flow path [ $\text{m}^3$ ]
$W$	Fracture width [m]
$z$	Axis orthogonal to the fracture
Greek	
$\rho_i$	Density (i=water w, but rock, R) [ $\text{kg}/\text{m}^3$ ]
$\tau_j$	Average travel time of the $j$ th flow path [s]
$\phi$	Porosity [-]
$\Phi_n$	Cumulative storage capacity at data point $n$
$\phi_j$	storage capacity of the $j$ th flow path

## REFERENCES

- Carslaw, H.W., and J.C. Jaeger. "Conduction of Heat in Solids." 2nd Ed., Oxford: *Clarendon Press*, (1959)
- Dean, C., Reimus, P., Oates, J., Rose, P., Newell, D., and Petty, S. "Laboratory experiments to characterize cation-exchanging tracer behavior for fracture surface area estimation at Newberry Crater, OR." *Geothermics*, 53, (2015), 213–224, doi:10.1016/j.geothermics.2014.05.011.
- Gringarten, A.C., and Sauty, J.P. "Theoretical study of heat extraction from aquifers from uniform regional flow." *Journal of Geophysical Research*, 80(35), (1975), 4956-4962.

- Gringarten, A. C., Witherspoon, P. A., and Ohnishi, Y. "Theory of heat extraction from fractured hot dry rock." *Journal of Geophysical Resources*, 80(8), (1975), 1120–1124. doi:10.1029/JB080i008p01120.
- Gunter, G.W., Finneran, J.M., Hartmann, D.J., and Miller, J.D. "Early determination of reservoir flow units using an integrated petrophysical method." *Society of Petroleum Engineers*, (1997) doi:10.2118/38679-MS.
- Lake, L.W. "Enhanced Oil Recovery." *Prentice Hall*. (1989).
- Lauwerier H.A. "The transport of heat in an oil layer caused by the injection of hot fluid." *Applied Scientific Research*, Section A, 5(2), (1955), 145–150.
- Pruess, K. and Doughty, C. "Thermal single-well injection-withdrawal tracer tests for determining fracture-matrix heat transfer area." *Proceedings: 35th Workshop on Geothermal Reservoir Engineering*, Stanford University, Stanford, CA (2010).
- Pruess, K. "TOUGH2—a general purpose numerical simulator for multiphase fluid and heat transfer." *Lawrence Berkeley Laboratory report LBL-29400*, Berkeley, CA, USA, (1991), 102 pp.
- Robinson, B.A. and Tester, J.W. "Dispersed fluid flow in fractured reservoirs: An analysis of tracer-determined residence time distributions." *Journal of Geophysical Research*, 89(B12), (1984), 10374–10384, doi:10.1029/JB089iB12p10374.
- Robinson, B.A., Tester, J.W., and Brown, L.F." Reservoir sizing using inert and chemically reacting tracers." *Society of Petroleum Engineers*, (1988). doi:10.2118/13147-PA
- Schmalz, J.P. and Rahme, H.D. "The variation of waterflood performance with variation in permeability profile." *Prod. Monthly*, 15(9), (1950) 9-12.
- Shan, C. and Pruess, K. "An analytical solution for slug tracer tests in fractured reservoirs." *Water Resources Research*, 41, W08502, (2005), doi:10.1029/2005WR004081.
- Shook, G.M. and Forsmann, J.H. "Tracer interpretation using temporal moments on a spreadsheet", *INL report 05-00400*, (2005).
- Shook, G.M., Pope, G.A., and Asakawa K. "Determining reservoir properties and flood performance from tracer test analysis." *Society of Petroleum Engineers*, (2009), doi:10.2118/124614-MS.
- Shook, G.M., and Suzuki, A. "Use of tracers and temperature to estimate fracture surface area for EGS reservoirs." *Geothermics*, 66 (2017) 40–47.
- Stiles, W.E. "Use of permeability distribution in waterflood calculations." *Journal of Petroleum Technology*, 1.01, 9-13, (1949).
- Stopa, J. and Wojnarowski, P. "Analytical model of cold water front movement into geothermal reservoir," *Geothermics*, 35(1), (2006), 59-69.
- Suzuki, A., Hashida, T., Li, K. and Horne, R.N. "Experimental tests of truncated diffusion in fault damage zones." *Water Resources Research*, 52, (2016), doi:10.1002/2016WR019017.